J|A|C|S
ARTICLES
Published on Web 12/10/2002

Monolayer Assemblies of a De Novo Designed 4-α-Helix Bundle Carboprotein and Its Sulfur Anchor Fragment on Au(111) Surfaces Addressed by Voltammetry and In Situ Scanning Tunneling Microscopy

Jesper Brask,[†] Hainer Wackerbarth,[†] Knud J. Jensen,*[,‡] Jingdong Zhang,[†] Ib Chorkendorff,[§] and Jens Ulstrup*[,†]

Contribution from the Department of Chemistry, Buildings 201 and 207, and Department of Physics and ICAT, Building 309, Technical University of Denmark, DK-2800 Lyngby, Denmark, and Department of Chemistry, The Royal Veterinary and Agricultural University, Thorvaldsensvej 40, DK-1871 Frederiksberg C, Denmark

Received July 9, 2002

Abstract: Mapping and control of proteins and oligonucleotides on metallic and nonmetallic surfaces are important in many respects. Electrochemical techniques based on single-crystal electrodes and scanning probe microscopies directly in aqueous solution (in situ SPM) have recently opened perspectives for such mapping at a resolution that approaches the single-molecule level. De novo design of model proteins has evolved in parallel and holds promise for testing and controlling protein folding and for new tailored protein structural motifs. In this report we combine these two strategies. We present a scheme for the synthesis of a new 4-α-helix bundle carboprotein built on a galactopyranoside derivative with a thiol anchor aglycon suitable for surface immobilization on gold. The carboprotein with thiol anchor in monomeric and dimeric (disulfide) form, the thiol anchor alone, and a sulfur-free 4-α-helix bundle carboprotein without thiol anchor have been prepared and investigated for comparison. Cyclic and differential pulse voltammetry (DPV) of the proteins show desorption peaks around −750 mV (SCE), whereas the thiol anchor desorption peak is at −685 mV. The peaks are by far the highest for thiol monomeric 4-α-helix bundle carboprotein and the thiol anchor. This pattern is supported by capacitance data. The DPV and capacitance data for the thiolated 4-α-helix bundle carboproteins and the thiol anchor hold a strong Faradaic *reductive* desorption component as supported by X-ray photoelectron spectroscopy. The desorption peak of the sulfur-free 4-α-helix bundle carboprotein, however, also points to a capacitive component. In situ scanning tunneling microscopy (in situ STM) of the thiol anchor discloses an adlayer with small domains and single molecules ordered in pin-striped supramolecular structures. In situ STM of thiolated 4-α-helix bundle carboprotein monomer shows a dense monolayer in a broad potential range on the positive side of the desorption potential. The coverage decreases close to this potential and single-molecule structures become apparent. The in situ STM contrast is also strengthened, indicative of a new redox-based tunneling mechanism. The data overall suggest that single-molecule mapping of natural and synthetic proteins on well-characterized surfaces by electrochemistry and in situ STM is within reach.

1. Introduction

Mapping of the structural organization and electron transfer (ET) function of proteins and other biomolecules, such as oligonucleotides, adsorbed on solid surfaces is crucial in several contexts. Fundamental contexts are adsorption patterns,[1−4] two-dimensional molecular interactions including phase transitions,[5−7] ET mechanisms of immobilized functional redox proteins and enzymes,[5,8−11] and mechanisms of coupled chemical and biocatalytic processes.[8,9,11] Biotechnological perspectives include protein−membrane interactions and drug delivery,[12,13] biological corrosion,[14] biocompatibility of metallic implantates,[15] and biofilms.[16] To this come areas under headings such as on-line "bioelectronic function", "biosensors" etc.,[8,9,17−20] covering

* Corresponding authors: kjj@kvl.dk and ju@kemi.dtu.dk.
[†] Department of Chemistry, Technical University of Denmark.
[‡] Department of Chemistry, The Royal Veterinary and Agricultural University.
[§] Department of Physics and ICAT, Technical University of Denmark.

(1) *Proteins at Interfaces II. Fundamentals and Applications*; Horbett, T. A., Brash, J. L., Eds.; ACS Symposium Series 602; American Chemical Society: Washington, DC, 1995.
(2) Tirrell, M.; Kokkoli, E.; Biesalski, M. *Surf. Sci.* **2002**, *500*, 61−82.
(3) Kasermo, B. *Surf. Sci.* **2002**, *500*, 656−677.
(4) Service, R. P. *Science* **1998**, *282*, 396−399.
(5) Zhang, J.; Chi, Q;, Kuznetsov, A. M.; Hansen, A. G.; Wackerbarth, H.; Christensen, H. E. M.; Andersen, J. E. T.; Ulstrup, J. *J. Phys. Chem. B* **2002**, *106*, 1131−1152.
(6) Castner, D. G.; Ratner, B. D. *Surf. Sci.* **2002**, *500*, 28−60.
(7) Nielsen, L. K.; Bjørnholm, T.; Mouritsen, O. G. *Nature* **2000**, *404*, 353.
(8) Shipway, A. N.; Willner, I. *Acc. Chem. Res.* **2001**, *34*, 421−432.
(9) Gilardi, G.; Fantuzzi, A. *Trends Biotechnol.* **2001**, *19*, 468−476.
(10) *Faraday Discussion Chem. Soc.* **2000**, *116*. Special issue on bioelectrochemistry.
(11) Jeuken, L. J. C.; Jones, A. K.; Chapman, S. K.; Cecchini, G.; Armstrong, F. A. *J. Am. Chem. Soc.* **2002**, *124*, 5702−5713.

10.1021/ja020943r CCC: $25.00

broadly bioelectrochemistry understood as interfacial electrochemical ET between metallic electrodes and adsorbed redox metalloproteins or other biomolecules. Electronic communication between the electrodes and the biomolecules can be controlled by electrode modification, covalent linking, and electromagnetic radiation where, for example, photoisomerization of molecular links to the electrode can be exploited.[8]

Ultimate goals of these efforts in areas broadly denoted as "bioelectronics" extend to bringing electronic control into true nanoscale and single-molecule levels. Other goals are to *combine* different nanoscale functions into biotechnological devices and *circuits*. Efforts along new lines are also needed, however, with the common notion of "single-molecule electronic technology". This implies first that interfacial *bioelectrochemical* ET should be combined with state-of-the-art *physical* electrochemistry, such as use of single-crystal electrode surfaces and in situ scanning probe techniques, particularly in situ scanning tunneling microscopy (STM).[21−23] The latter images single-molecule function directly in the biological aqueous buffer media. A second approach addresses systematically *molecular* structure−function relations, where secondary and tertiary protein-folding and stability features can be controlled and tailor-made, and the resulting bioelectrochemical function monitored.

In this report we combine these two approaches, based on de novo designed 4-α-helix bundle (4HB) carboprotein structures.[24−26] These are intermediate-size structures simplified compared with natural proteins. Their secondary and tertiary structural elements can be varied systematically, enabling new levels of detail in molecular structure−function relations. Several groups have developed synthetic 4HB proteins by using different strategies.[27−31] Two of the present authors have introduced the use of monosaccharides as templates for the de novo design of 4HB proteins denoted as carboproteins.[24−26] Such a 4HB carboprotein and its anchor fragment for protein immobilization on Au-electrode surfaces are target molecules in the present report. The 4HB carboprotein and its partial molecular structure are brought to immobilization on *single-crystal* Au(111) electrodes. This enables characterization of the protein and partial structure monolayers by electrochemical approaches based on atomically planar electrode surfaces. Molecular monolayer characterization includes cyclic (CV) and differential pulse voltammetry (DPV), interfacial capacitance data, X-ray photoelectron spectroscopy (XPS), and in situ STM directly in aqueous buffer media. Such combinations have only recently been introduced in the context of natural or synthetic macromolecules.[5,32−38] The present investigation shows that the combination of totally synthetic proteins with state-of-the-art physical electrochemistry indeed holds promise for addressing biomolecular structure and function at the single-molecule and supramolecular levels.

2. Experimental Section

2.a. Synthesis of Carboproteins and Anchor Molecule. 2.a.1. General Procedures. Tritylmercaptoacetic acid was prepared in 76% yield from chloroacetic acid.[39] 4-Aminophenyl α-D-Gal*p*, **1**, was prepared in 92% yield by catalytic hydrogenation of 4-nitrophenyl α-D-Gal*p*.[40] Boc_2NOCH_2COOH (Boc_2-Aoa-OH) was prepared in 77% yield from Boc-Aoa-OH.[25] For synthetic details for peptide aldehyde Ac-YEELLKKLEELLKKAG-H, **5**, and the 4HB carboprotein without anchor, **12**, refer to ref 41. ^1H and ^{13}C NMR spectra were recorded at 500 and 125.7 MHz, respectively, on a Varian Unity Inova 500 spectrometer. Electrospray ionization mass spectrometry (ESI MS) was performed on a Micromass LCT mass spectrometer. For further general procedures and instrumentation, see refs 25 and 42.

2.a.2. 4-(Tritylmercaptoacetamide)phenyl α-D-Gal*p*, 2. $TrSCH_2$-COOH (213 mg, 0.64 mmol) was dissolved in dimethylformamide (DMF) (10 mL), and PyBOP (331 mg, 0.64 mmol), HOBt (97 mg, 0.64 mmol), and DIPEA (218 μL, 1.27 mmol) were added. After 5 min, compound **1** (157 mg, 0.58 mmmol) was added. The dark solution was stirred for 18 h and then concentrated to dryness, dissolved in MeCN (3 mL), and purified by prep. C_{18} RP-HPLC. Product **2** was obtained as a white solid. Yield 300 mg; 88%. m.p. 115−117 °C. ^1H NMR (DMSO-d_6, D_2O-exch), δ: 7.4−7.2 (m, 15H, Tr), 7.25 (d, 8.8 Hz, 2H, aryl), 6.98 (d, 8.8 Hz, 2H, aryl), 5.29 (d, 2.8 Hz, 1H, H-1), 3.8−3.7 (m, 4H, H-2/3/4/5), 3.50 (dd, 6.5 Hz, 11.4 Hz, 1H, H-6a), 3.4−3.3 (m, 1H, H-6b), 2.99 (s, 2H, CH_2S). ^{13}C NMR (DMSO-d_6), δ: 166.9 (NHCO), [154.5, 134.1, 121.6, 118.4] (aryl, OPhNH), [145.2, 130.3, 129.3, 128.0] (aryl, Tr), 99.8 (C-1), 73.2 (C-5), [70.4, 69.6, 69.1] (C-2/3/4), 67.3 (CPh_3), 61.4 (C-6), 38.1 (CH_2S).

2.a.3. 4-(Tritylmercaptoacetamide)phenyl 2,3,4,6-tetra-*O*-(Boc_2-Aoa)-α-D-Gal*p*, 3. Compound **2** (80 mg, 0.14 mmol) and Boc_2-Aoa-OH (238 mg, 0.82 mmol) were dissolved in pyridine/DCM (1:1, 4 mL). DMAP (10 mg, 0.082 mmol) and *N*,*N*′-diisopropylcarbodiimide (DIPCDI) (126 μL, 0.81 mmol) were added. After 30 min, TLC (EtOAc−hexane, 2:3) showed several products and additional DIPCDI

(12) Lasic, D. D. *Liposomes*: *From Physics to Applications*, 2nd ed.; Elsevier: Amsterdam, 1995.
(13) Storm, G.; Crommelin, D. J. A. *Pharm. Sci. Technol. Today* **1998**, *1*, 19−31.
(14) Telegdi, J.; Keresztes, Z.; Pálinkas, G.; Kálmán, E.; Sand, W. *Appl. Phys. A* **1998**, *66*, S639−S642.
(15) Walavaara, B.; Askendal, A.; Lundström, I.; Tengwall, P. *J. Biomater. Sci. Forum* **1998**, *8*, 41−48.
(16) Telegdi, J.; Shaban, A.; Beczner, J.; Keresztes, Z.; Kálmán, E. *Mater. Sci. Forum* **1998**, *289*, 77−82.
(17) Eggins, B. *Biosensors. An Introduction*; Wiley: Chichester, UK, 1997.
(18) Wang, J. *Electroanalysis* **2001**, *13*, 983−988.
(19) Piedade, J. A. P.; Fernandes, I. R.; Oliveira-Brett, A. M. *Bioelectrochemistry* **2002**, *56*, 81−83, and references there.
(20) Palecek, E.; Fojta, M.; Jelen, F. *Bioelectrochemistry* **2002**, *56*, 85−90.
(21) *Nanoscale Probes of the Solid/Liquid Interface*; Gewirth, A. A., Siegenthaler, H., Eds.; Kluwer: Dordrecht, 1995.
(22) *Imaging of Surfaces and Interfaces*; Lipkowski, J., Ross, P. N., Eds.; Wiley-VCH: New York, 1999.
(23) Danilov, A. I. *Russ. Chem. Rev.* **1995**, *64*, 767−781.
(24) Jensen, K. J.; Barany, G. *J. Pept. Res.* **2000**, *56*, 3−11.
(25) Brask, J.; Jensen, K. J. *J. Pept. Sci.* **2000**, *6*, 290−299.
(26) Brask, J.; Jensen, K. J. *Bioorg. Med. Chem. Lett.* **2001**, *11*, 697−700.
(27) DeGrado, W. F.; Summa, C. M.; Pavone, V.; Nastri, F.; Lombardi, A. *Annu. Rev. Biochem.* **1999**, *68*, 779−819.
(28) Choma, C. T.; Lear, J. D.; Nelson, M. J.; Dutton, P. L.; Robertson, D. E.; DeGrado, W. F. *J. Am. Chem. Soc.* **1994**, *116*, 856−865.
(29) Robertson, D. E.; Farid, R. S.; Moser, C. C.; Urbauer, J. L.; Mulholland, S. E.; Pidikiti, R.; Lear, J. D.; Wand, A. J.; DeGrado, W. F.; Dutton, P. L. *Nature* **1994**, *368*, 425−432.
(30) Rau, H. K.; DeJonge, N.; Haehnel, W. *Angew. Chem., Int. Ed.* **2000**, *39*, 250−253.
(31) Mutter, M.; Vuilleumier, S. *Angew. Chem., Int. Ed. Engl.* **1989**, *28*, 535−554.
(32) Andersen, J. E. T.; Møller, P.; Pedersen, M. V.; Ulstrup, J. *Surf. Sci.* **1995**, *325*, 193−205.
(33) Zhang, J.; Chi, Q.; Dong, S.; Wang, E. *Bioelectrochem. Bioenerg.* **1996**, *39*, 267−274.
(34) Andersen, J. E. T.; Olesen, K. G.; Danilov, A. I.; Foverskov, C. E.; Møller, P.; Ulstrup, J. *Bioelectrochem. Bioenerg.* **1997**, *44*, 57−63.
(35) Friis, E. P.; Andersen, J. E. T.; Madsen, L. L.; Møller, P.; Ulstrup, *J. Electroanal. Chem.* **1997**, *431*, 35−38.
(36) Friis, E. P.; Andersen, J. E. T.; Kharkats, Yu. I.; Kuznetsov, A. M.; Nichols, R. J.; Zhang, J.; Ulstrup, J. *Proc. Natl. Acad. Sci. U.S.A.* **1999**, *96*, 1379−1384.
(37) Chi, Q.; Zhang, J.; Friis, E. P.; Anderen, J. E. T.; Ulstrup, J. *Electrochem. Commun.* **1999**, *1*, 91−96.
(38) Chi, Q.; Zhang, J.; Nielsen, J. U.; Friis, E. P.; Chorkendorff, I.; Canters, G. W.; Andersen, J. E. T.; Ulstrup, J. *J. Am. Chem. Soc.* **2000**, *122*, 4047−4055.
(39) Bell, A. B.; Hughes, D. W.; Lock, C. J. L.; Valliant, J. F. *Can. J. Chem.* **1996**, *74*, 1503−1511.
(40) Westphal, O.; Feier, H. *Chem. Ber.* **1956**, *89*, 582−588.
(41) Brask, J.; Dideriksen, J. M.; Nielsen, J.; Jensen, K. J., submitted.
(42) Boas, U.; Brask, J.; Christensen, J. B.; Jensen, K. J. *J. Comb. Chem.* **2002**, *4*, 223−228.

(126 μL) was added. After further 30 min, TLC (EtOAc−hexane, 2:3) showed one major component with R_f 0.65. The suspension was concentrated to dryness and CH_3CN (5 mL) was added. Solid *N*,*N*′-diisopropylurea was filtered off and the mixture was purified by prep. C_{18} RP-HPLC. Product **3** was obtained as a viscous oil, which crystallized when a solution in EtOH was poured over ice water. The crystals were filtered off and dried in vacuo. Yield 142 mg; 62%. m.p. 80−83 °C. ^{1}H NMR ($CDCl_3$), δ: 7.5−7.2 (m, 15H, Tr), 7.20 (d, 9.0 Hz, 2H, aryl), 6.93 (d, 9.0 Hz, 2H, aryl), 5.76 (d, 3.3 Hz, 1H, H-1), 5.70 (dd, 10.7 Hz, 3.2 Hz, 1H, H-3), 5.59 (d, 3.4 Hz, 1H, H-4), 5.27 (dd, 11.1 Hz, 3.9 Hz, 1H, H-2), 4.7−4.4 (m, 9H, CH_2 Aoa/H-5), 4.24 (dd, 11.3 Hz, 6.5 Hz, 1H, H-6a), 4.20 (dd, 11.2 Hz, 6.4 Hz, 1H, H-6b), 3.29 (s, 2H, CH_2S), [1.55, 1.54, 1.51, 1.50] (singlets, 72H, Boc). ^{13}C NMR ($CDCl_3$), δ: [167.5, 167.3, 167.1, 167.0] (CO Aoa), 166.5 (NHCO), [153.3, 133.7, 122.0, 118.0] (aryl, OPhNH), [150.7, 150.7, 150.6, 150.5] (CO Boc), [144.5, 130.1, 129.0, 127.9] (aryl, Tr), 95.9 (C-1), [85.2, 85.2, 85.1, 85.0] ($C(CH_3)_3$), [72.8, 72.6, 72.5] (CH_2 Aoa/CPh_3), [69.4, 69.0, 68.3, 67.6] (C-2/3/4/5), 62.5 (C-6), 37.2 (CH_2S), [28.8, 28.7, 28.7] ($C(CH_3)_3$).

2.a.4. 4-(Mercaptoacetamide)phenyl 2,3,4,6-tetra-*O*-(Aoa)-α-D-Gal*p*, 4. Compound **3** (33 mg, 20 μmol) was deprotected in trifluoroacetic acid (TFA)/DCM/Et_3SiH (1:1:0.1, 4.2 mL) for 1 h. The colorless solution was then concentrated to dryness, dissolved in DCM (2 mL), and extracted with H_2O (4 × 2 mL). The combined aqueous phases were freeze-dried to give template **4** as a white powder. Yield 22 mg; 102% (incl. 4× TFA). ^{1}H NMR (D_2O), δ: 7.38 (d, 8.8 Hz, 2H, aryl), 7.12 (d, 8.7 Hz, 2H, aryl), 6.02 (d, 3.5 Hz, 1H, H-1), 5.81 (dd, 10.7 Hz, 3.0 Hz, 1H, H-3), 5.74 (d, 2.9 Hz, 1H, H-4), 5.54 (dd, 10.5 Hz, 3.8 Hz, 1H, H-2), 4.8−4.3 (m, 11H, CH_2 Aoa/H-5/6), 3.35 (s, 2H, CH_2S). ESI MS, Calcd for $C_{22}H_{31}N_5O_{15}S$: 637.15 Da. Found: *m*/*z* 675.97 $[M + K]^+$, 660.01 $[M + Na]^+$, 638.15 $[M+H]^+$.

2.a.5. 4HB-carboprotein, 6. Template **4** (16 mg, 14.6 μmol) was dissolved in H_2O (2.1 mL). Peptide **5** (10 mg, 4.2 μmol) was dissolved in MeCN/1 M acetate buffer, pH 4.76 (1:1, 2 mL). To initiate the reaction, 100 μL (0.70 μmol) of the template solution was transferred to the peptide solution. After 3 h, the mixture was directly injected to prep. C_4 RP-HPLC. After lyophilization of fractions containing product, carboprotein **6** was obtained as a white powder. Yield 8 mg; 113% (incl. 32× TFA). ESI MS, Calcd for $C_{382}H_{631}N_{85}O_{115}S$: 8287 Da (average isotope). Found: *m*/*z* 1656.84 $[M + 5H]^{5+}$, 1381.83 $[M + 6H]^{6+}$, 1184.86 $[M + 7H]^{7+}$, 1036.96 $[M + 8H]^{8+}$, 921.86 $[M + 9H]^{9+}$, 829.76 $[M + 10H]^{10+}$, 754.38 $[M + 11H]^{11+}$.

2.a.6. 4-(Mercaptoacetamide)phenyl α-D-Gal*p* disulfide, 7. Compound **2** (197 mg, 0.34 mmol) was deprotected with TFA/DCM/Et_3SiH (1:1:0.1, 21 mL) for 30 min. The colorless solution was then concentrated to dryness, suspended in Et_2O (50 mL), and extracted with H_2O (2 × 25 mL). DMSO (5 mL) was added to the aqueous phase. The solution was stirred for 18 h in an open flask, and then purified by prep. C_{18} RP-HPLC. Product **7** was obtained as white needles. Yield 86 mg; 75%. m.p. 248−250 °C (decomp.). ^{1}H NMR (DMSO, D_2O-exch.), δ: 7.46 (dd, 1.8 Hz, 6.5 Hz, 4H, aryl), 7.02 (dd, 2.2 Hz, 6.8 Hz, 4H, aryl), 5.30 (d, 2.3 Hz, 2H, H-1), 3.8−3.3 (m, 16H, H-2/3/4/5/6/CH_2S). ^{13}C NMR (DMSO), δ: 167.5 (NHCO), [154.6, 134.0, 121.8, 118.6] (aryl), 99.8 (C-1), 73.2 (C-5), [70.4, 69.6, 69.1] (C-2/3/ 4), 61.4 (C-6), 44.1 (CH_2S).

2.a.7. 4-(Mercaptoacetamide)phenyl 2,3,4,6-tetra-*O*-(Boc_2-Aoa)-α-D-Gal*p* disulfide, 8. Compound **7** (80 mg, 0.12 mmol) and Boc_2-Aoa-OH (338 mg, 1.16 mmol) were suspended in pyridine/DCM (1:1, 4 mL). DMAP (14 mg, 0.12 mmol) and DIPCDI (180 μL, 1.16 mmol) were added. Additional DIPCDI (2 × 180 μL) was added in two portions during the next 4 h,. After a further 16 h, the suspension was concentrated to dryness and CH_3CN (5 mL) was added. Solid *N*,*N*′-diisopropylurea was filtered off and the mixture was purified by prep. C_{18} RP-HPLC. Product **8** was obtained as a clear, colorless oil. Yield 86 mg; 26%. ^{1}H NMR (DMSO), δ: 7.56 (d, 8.8 Hz, 4H, aryl), 7.04 (d, 8.8 Hz, 4H, aryl), 5.67 (d, 3.4 Hz, 2H, H-1), 5.6−5.5 (m, 4H, H-3/4), 5.13 (dd, 10.7 Hz, 3.5 Hz, 2H, H-2), 4.8−4.4 (m, 18H, CH_2 Aoa/H-5), 4.23 (dd, 11.5 Hz, 7.0 Hz, 2H, H-6a), 4.15 (dd, 11.4 Hz, 5.3 Hz, 2H, H-6b), 3.72 (s, 4H, CH_2S), [1.46, 1.46, 1.42, 1.40] (singlets, 144H, Boc). ^{13}C NMR (DMSO), δ: [167.9, 167.9, 167.7, 167.1] (CO Aoa), [153.1, 135.9, 121.8, 119.5] (aryl), [150.6, 150.5, 150.5, 150.5] (CO Boc), 96.8 (C-1), [84.9, 84.8, 84.8] ($C(CH_3)_3$), 73.0 (CH_2 Aoa), [69.9, 68.3, 67.9] (C-2/3/4/5), 44.1 (CH_2S), [28.7, 28.7, 28.7] ($C(CH_3)_3$).

2.a.8. 4-(Mercaptoacetamide)phenyl 2,3,4,6-tetra-*O*-(Aoa)-α-D-Gal*p* disulfide, 9. Compound **8** (75 mg, 26 μmol) was deprotected in TFA/DCM (1:1, 4 mL) for 30 min. The colorless solution was then concentrated to dryness, dissolved in H_2O/CH_3CN (10:0.2, 10 mL), and lyophilized to give template **9** as a white powder. Yield 56 mg; 98% (incl. 8× TFA). ^{1}H NMR (DMSO, D_2O-exch.), δ: 7.54 (d, 8.9 Hz, 4H, aryl), 7.07 (d, 9.3 Hz, 4H, aryl), 5.75 (d, 3.5 Hz, 2H, H-1), 5.6−5.5 (m, 4H, H-3/4), 5.25 (dd, 10.1 Hz, 3.7 Hz, 2H, H-2), 4.7−4.3 (m, 18H, CH_2 Aoa/H-5), 4.23 (dd, 11.5 Hz, 7.1 Hz, 2H, H-6a), 4.16 (dd, 11.0 Hz, 5.1 Hz, 2H, H-6b). ESI MS, Calcd for $C_{44}H_{60}N_{10}O_{30}S_2$: 1272.29 Da. Found: *m*/*z* 1295.42 $[M + Na]^+$, 1273.42 $[M+H]^+$.

2.a.9. 4HB-Carboprotein Dimer, 10. Template **9** (11 mg, 5.2 μmol) was dissolved in DMSO (1 mL). Peptide **5** (8 mg, 3.4 μmol) was dissolved in 0.1 M acetate buffer, pH 4.76 (4 mL). To initiate reaction, 54 μL (0.28 μmol) of the template solution was transferred to the peptide solution. After 3 h, the mixture was directly injected to prep. C_4 RP-HPLC. After lyophilization of fractions containing product, carboprotein **10** was obtained as a white powder. Yield 6 mg; 100% (incl. 32× TFA). ESI MS, Calcd for $C_{764}H_{1260}N_{170}O_{230}S_2$: 16571 Da (average isotope). Found: *m*/*z* 1656.50 $[M + 10H]^{10+}$, 1506.76 $[M + 11H]^{11+}$, 1381.64 $[M + 12H]^{12+}$, 1275.52 $[M + 13H]^{13+}$, 1184.66 $[M + 14H]^{14+}$, 1105.77 $[M + 15H]^{15+}$, 1036.82 $[M + 16H]^{16+}$.

2.a.10. *N*-Phenyl-mercaptoacetamide disulfide, 11. Tritylmercaptoacetic acid (200 mg, 0.60 mmol) was dissolved in DCM (10 mL). Aniline (60 μL, 0.66 mmol) was added, followed by DIPCDI (139 μL, 0.90 mmol). After 18 h, the mixture was evaporated to dryness and the residue dissolved in TFA/DCM/Et_3SiH (1:1:0.1, 10.5 mL). After 30 min, the clear solution was again evaporated to dryness. The residue was dissolved in DMSO/MeCN (1:1, 4 mL) and neutralized with 1 M $KHCO_3$ (1 mL). The resulting suspension was stirred in an open flask for 18 h, before being concentrated to 1 mL, dissolved in MeCN (5 mL), and injected to prep. C_{18} RP-HPLC. Concentration of fractions gave the title compound as white crystals. Yield 74 mg; 74%. m.p. 157−159 °C (lit. 161−163 °C[43]). ^{1}H NMR (CD_3OD), δ: 7.57 (d, 8.4 Hz, 4H, aryl), 7.31 (t, 7.3 Hz, 4H, aryl), 7.11 (t, 7.5 Hz, 2H, aryl), 3.68 (s, 4H, $COCH_2S$). ESI MS, Calcd for $C_{16}H_{16}N_2O_2S_2$: 332.07 Da. Found: *m*/*z* 355.27 $[M + H]^+$, 333.30 $[M + Na]^+$.

2.b. Analytical Gel Filtration. Gel filtration was performed with a Superdex 75 HR 10/30 column (Amersham Biosciences, Sweden) connected to a Waters HPLC system (600 control unit, 996 PDA detector, 717 Plus autosampler, Millenium 32 control software). A 100-μL carboprotein sample was injected from a 2 mg/mL solution in 10 mM phosphate, pH 7.0 buffer. Elution buffer was 50 mM phosphate, 100 mM NaCl, pH 7.0. Samples were eluted with 1 mL/min flow rate and detected by UV absorption at 215 nm. The column was calibrated with albumin, ovalbumin, chymotrypsinogen A, ribonuclease A, aprotinin, and vitamin B_{12}.

2.c. Circular Dichroism Spectroscopy. CD spectra were recorded on a Jasco J-710 instrument at 20 °C (Jasco, Inc., USA). Carboprotein solutions were 20 μM (carboprotein **6**) and 10 μM (carboprotein **10**) in 10 mM NaH_2PO_4, pH 7.0. The carboprotein concentration was determined gravimetrically. The mean residue ellipticity was calculated as $[\theta] = \theta/(10 \times l \times c \times n)$, where θ [mdeg] is the measured ellipticity, l [cm] the path length, c [mol L^{-1}] the carboprotein concentration, and n the number of amino acid residues in the carboprotein, that is, 60 for **6** or 120 for **10**.

2.d. Preparation of Samples for Voltammetry, In Situ STM, and XPS. Single-crystal gold bead electrodes for voltammetry and capaci-

(43) Schimelpfenig, C. W. *J. Org. Chem.* **1962**, *27*, 3323−3324.

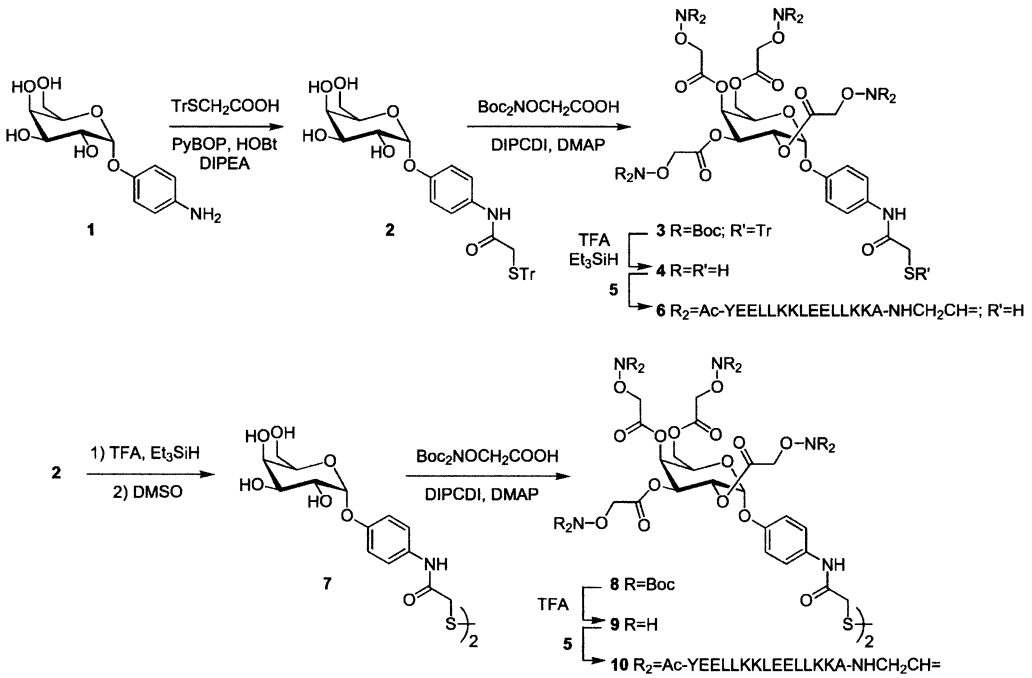

Figure 1. Chemical synthesis of 4HB-carboprotein monomer **6** and 4HB-carboprotein dimer **10**. Ligation of hexadecapeptide aldehyde **5** to aminooxy-functionalized templates **4** and **9** proceeded quantitatively by oxime formation.

tance measurements were prepared by the method of Clavilier[44] and Hamelin.[45] A Au(111) disk (Surface Preparation Laboratory, The Netherlands, www.surface-prep-lab.com, 12-mm diameter, 1 mm thick) was used as substrate in STM and XPS. Before use, the electrodes were electropolished in 0.1 M H_2SO_4 (10 V, followed by soaking in 1 M HCl) and annealed in a hydrogen flame. The disk substrate was then cooled to room temperature, while the bead was kept for 1 min above a Millipore water surface, followed by immersion into the water. Substrate and bead electrodes were finally transferred to aqueous buffer solution of the carboprotein or anchor molecule for several hours. The carboprotein solutions were 0.23 mM protein in 0.1 M K_2HPO_4/KH_2PO_4 buffer (pH 6.9, 18 h), the anchor fragment 15 mM solution in methanol (several hours). The samples were thoroughly rinsed with Millipore water.

2.e. Voltammetry and Capacitance Measurements. Glassware in electrochemical and in situ STM measurements was cleaned as reported.[37] The hang meniscus method was used in voltammetric and capacitance measurements.[37,38] CV, DPV, and interfacial capacitances were recorded using an Autolab system (Eco Chemie, The Netherlands) controlled by the general-purpose software. Parameters in DPV and capacitance measurements were the same as previously[37,38] (10 mV s^{-1} scan rate and 4.05 mV step potential in DPV, 100 Hz and 5 mV modulation amplitude in capacitance measurements). A coiled bright platinum wire and a saturated calomel electrode (SCE) were used as counter and reference electrode, respectively. All potentials refer to the SCE. Solutions were deoxygenated by purified argon (Chrompack, 5N) before use and an argon atmosphere maintained above the solutions during experimental recordings.

2.f. In Situ STM. A PicoSPM instrument (Molecular Imaging Co., USA) with a bipotentiostat for independent control of substrate and tip potential, and in-house-built three-electrode KEL-F cells were used, in the constant-current mode. The substrate was a Au(111) disk, compare with above. Reference and counter electrodes were platinum wires; 10 mM phosphate (pH 6.8) was supporting electrolyte. Tungsten tips were prepared and coated as described.[38]

2.g. XPS Measurements. The XPS spectra were recorded using a Perkin−Elmer surface analysis system (Physical Electronic Industries, Inc., USA) equipped with a multichannel detector. A Mg-anode operated at 200 W was used to generate X-rays. The pressure in the chamber during data acquisition was less than 1×10^{-9} Torr. The pass energy was either 25.0 or 50.0 eV. All spectra were acquired at room temperature and are referenced to the Au($4f_{7/2}$) line at 84.00 eV.

3. Results

3.a. Synthesis and Structure of Carboprotein and Anchor Fragment. Commercially available 4-nitrophenyl α-D-galactopyranoside (α-D-Gal*p*) was chosen as starting material for the template synthesis, as reduction of the nitro group to an amine allowed functionalization of the aglycon of the monosaccharide. Taking advantage of the selectivity of the PyBOP coupling reagent for forming amide bonds, chemoselective coupling of $TrSCH_2COOH$ to 4-aminophenyl α-D-Gal*p*, **1**, gave 4-(tritylmercaptoacetamide)phenyl α-D-Gal*p*, **2**, in 88% yield (Figure 1). Next, the four hydroxyls were acylated with Boc_2-Aoa-OH, using a previously developed protocol,[25] to give protected template **3** in 62% yield. An alternative strategy, in which Boc_2-Aoa-OH acylation of 4-nitrophenyl α-D-Gal*p* was followed by reduction of the nitro group, proved unsuccessful, because reduction by catalytic hydrogenation lead to a complex mixture. Treatment of **3** with TFA leads to facile and quantitative removal of all protecting groups (eight Boc and one Tr). Triethylsilane was added to scavenge the liberated trityl cations, and thus to prevent reattachment of the protecting group onto the thiol upon concentration of the mixture.[46] The lyophilized deprotected template **4** was dissolved in a mixture of MeCN and aqueous acetate buffer, pH 4.76, together with 50% excess of the hexadecapeptide aldehyde Ac-YEELLKKLEELLKKAG-H, **5**. The 4HB-carboprotein monomer, **6**, was formed during 3 h under Ar by chemoselective oxime ligation[47] and was obtained in quantitative yield after prep. HPLC. The peptide aldehyde **5** was synthesized on solid-phase by a BAL strategy.[42,48]

(44) Clavilier, J.; Faure, R.; Guinet, G.; Durand, R. *J. Electroanal. Chem.* **1980**, *107*, 205−209.
(45) Hamelin, A. *J. Electroanal. Chem.* **1996**, *411*, 1−11.
(46) Pearson, D. A.; Blanchette, M.; Baker, M. L.; Guindon, C. A. *Tetrahedron Lett.* **1989**, *30*, 2739−2742.

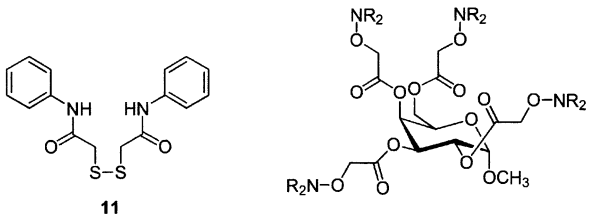

Figure 2. The two reference structures, *N*-phenyl-mercaptoacetamide disulfide, **11**, and 4HB carboprotein without thiol anchor, **12**.

Because of the difficulties with keeping **6** in the reduced form, that is, to avoid disulfide formation, the 4HB-carboprotein dimer, **10**, was prepared (Figure 1). Hence, **2** was treated with TFA to deprotect the thiol group. The intermediate was extracted into water, to which DMSO was added to facilitate oxidation to the disulfide. 4-(Mercaptoacetamide)phenyl α-D-Gal*p* disulfide, **7**, was formed over 18 h and purified to a white solid in 75% yield. Boc_2-Aoa-OH functionalization of all eight hydroxyl groups proceeded, using the same protocol as for the monomer, to give the desired protected template **8** in a modest yield of 26%. Next, **8** was quantitatively deprotected with TFA to give template **9**, which subsequently was ligated to peptide aldehyde **5** to give the 4HB-carboprotein dimer, **10**, likewise in quantitative yield. The ligation reaction was performed in aqueous acetate buffer pH 4.76, containing a trace of DMSO, with 50% excess of peptide aldehyde **5**.

The thiol anchor aglycon of carboproteins **6** and **10** was prepared as the disulfide **11** to provide a reference compound in the electrochemical studies of the carboproteins. $TrSCH_2$-COOH and aniline were coupled with DIPCDI, after which the trityl group was removed with TFA and Et_3SiH scavenging, and the resulting thiol oxidized to the disulfide with DMSO. The desired compound, *N*-phenyl-mercaptoacetamide disulfide, **11**, was obtained as a white solid in 74% overall yield (Figure 2).

Likewise, the 4HB carboprotein without thiol anchor, **12**, was prepared to provide a sulfur-free reference structure (Figure 2). Preparation of **12** is reported elsewhere.[41] Carboproteins **6** and **10** were characterized by ESI MS (Figure 3) and analytical gel filtration (Figure 4). In both cases MS gave a series of multiply protonated species, which could be deconvoluted to the putative molecular ion, shown in the insets of Figure 3. For both monomer and dimer carboprotein the correct mass was found, 8287 and 16 571 Da, respectively. Gel filtration clearly illustrated the size difference of the two structures. By calibrating the column with a series of globular proteins of known size, the size of the 4HB-carboprotein monomer **6** could be estimated to 10 707 Da. Similar for the 4HB-carboprotein dimer **10**, a size estimate of 22 064 Da was obtained. Hence, the dimer was found to be slightly more than twice the size of the monomer. Nonglobular shapes of the carboproteins can potentially explain the difference between these results and the masses determined by MS. The elution profiles (inset in Figure 4) showed close to symmetrical peak shapes. However, the profile of the later eluting 4HB-carboprotein monomer **6** revealed some disulfide formation due to air-oxidation of the structure in the pH 7.0 phosphate buffer. Finally, carboproteins **6** and **10** were characterized by CD spectroscopy (Figure 5). The spectra of both structures showed a high content of α-helix. Based on the mean residue ellipticity at 222 nm, the helicity was calculated to 57% for **6** and 61% for **10**.[49]

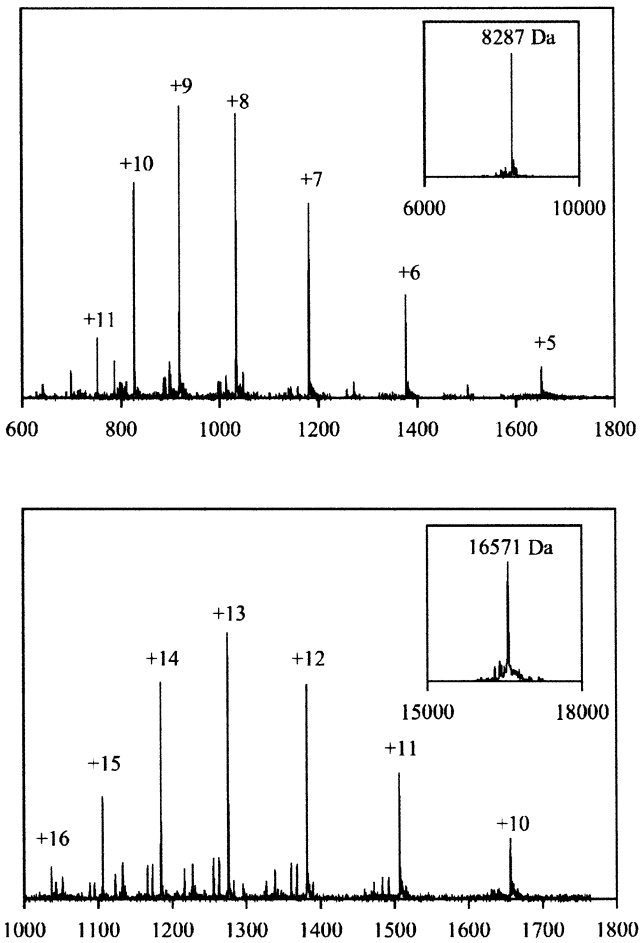

Figure 3. ESI-MS of 4HB-carboprotein monomer **6** (top) and 4HB-carboprotein dimer **10** (bottom). The insets show the deconvoluted spectra (MassLynx transform algorithm). Calculated molecular masses (average isotope distribution) for the two carboproteins are 8287 and 16 571 Da, respectively.

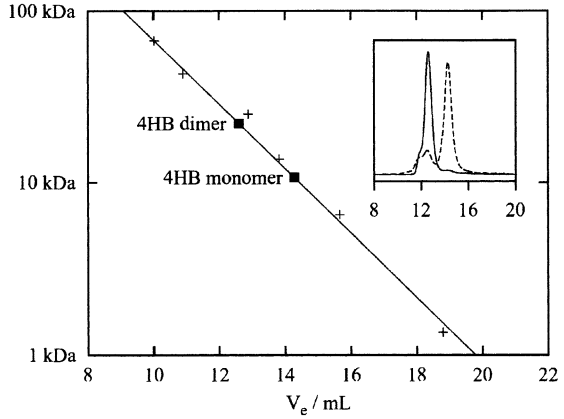

Figure 4. Gel filtration (size exclusion chromatography) of 4HB-carboprotein monomer **6** and 4HB-carboprotein dimer **10**. The linear correlation between elution volume (V_e) and log MW was established from calibration with albumin, ovalbumin, chymotrypsinogen A, ribonuclease A, aprotinin, and vitamin B_{12}. The inset shows the elution profiles of **6** (dashed line) and **10** (fully drawn line).

(47) Rose, K. *J. Am. Chem. Soc.* **1994**, *116*, 30−33.
(48) Jensen, K. J.; Alsina, J.; Songster, M. F.; Vágner, J.; Albericio, F.; Barany, G. *J. Am. Chem. Soc.* **1998**, *120*, 5441−5452.

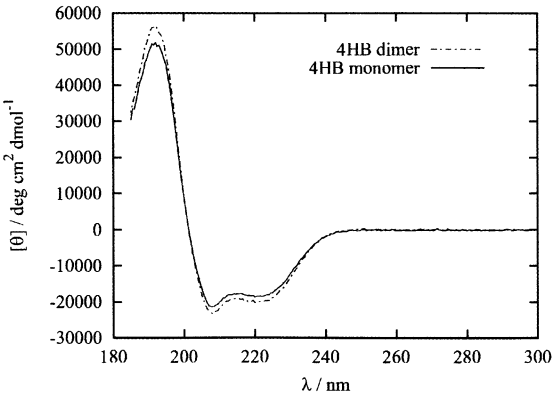

Figure 5. CD spectra of 4HB-carboprotein monomer **6** and 4HB-carboprotein dimer **10**, 10 mM phosphate buffer, pH 7.0, 20 °C.

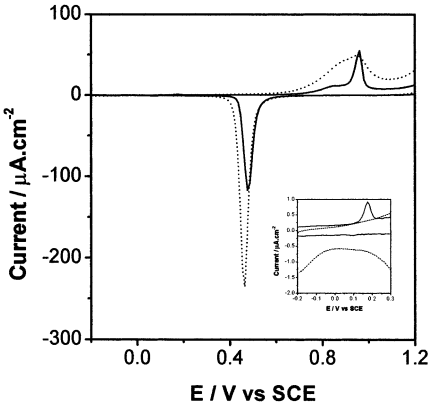

Figure 6. Cyclic voltammograms of Au(111) in 100 mM phosphate, pH 6.9. Fully drawn line, bare electrode; dashed line, Au(111) after adsorption of 4HB-carboprotein **6**. Scan rate 10 mV s^{-1}. Scan range: −0.2 to 1.2 V. The inset shows an enlarged view of the voltammogram in the potential range of Au(111)-surface reconstruction, −0.2 to 0.3 V.

3.c. Cyclic and Differential Pulse Voltammetry. Voltammetric data for reductive desorption and interfacial capacitances were recorded for the 4HB-carboprotein **6**, the 4HB-carboprotein dimer **10**, the 4HB-carboprotein without thiol anchor **12**, and for the anchor fragment **11**. The carboproteins are stable at acidic and neutral pH. Reductive desorption is usually effected under basic conditions to avoid electrochemical dihydrogen evolution. This interference was of minor importance in the present investigation. All voltammetric and capacitance data were recorded using 100 mM phosphate buffer (pH 6.9) where the proteins are stable.

The fully drawn lines in Figure 6 show cyclic voltammograms of Au(111) in the potential ranges of Au-oxide formation and reduction and lifting of the surface reconstruction (inset). The dashed lines show voltammograms in the same potential ranges when the 4HB-carboprotein **6** is adsorbed. Oxidation is strongly enhanced and the reconstruction peak disappears on carboprotein adsorption, indicative of significant surface coverage. This is substantiated by the data in Figures 7−9. Figure 7A, B shows differential pulse voltammograms in the reductive desorption region of the anchor fragment **11** (Figure 7A) and the three different forms of the 4HB carboprotein (Figure 7B) in 0.1 M phosphate buffer, pH 6.9. Figure 7C shows cyclic voltammograms of the 4HB-carboprotein thiol monomer **6**. The DPV of anchor **11** displays a strong peak at −685 mV, with a shoulder

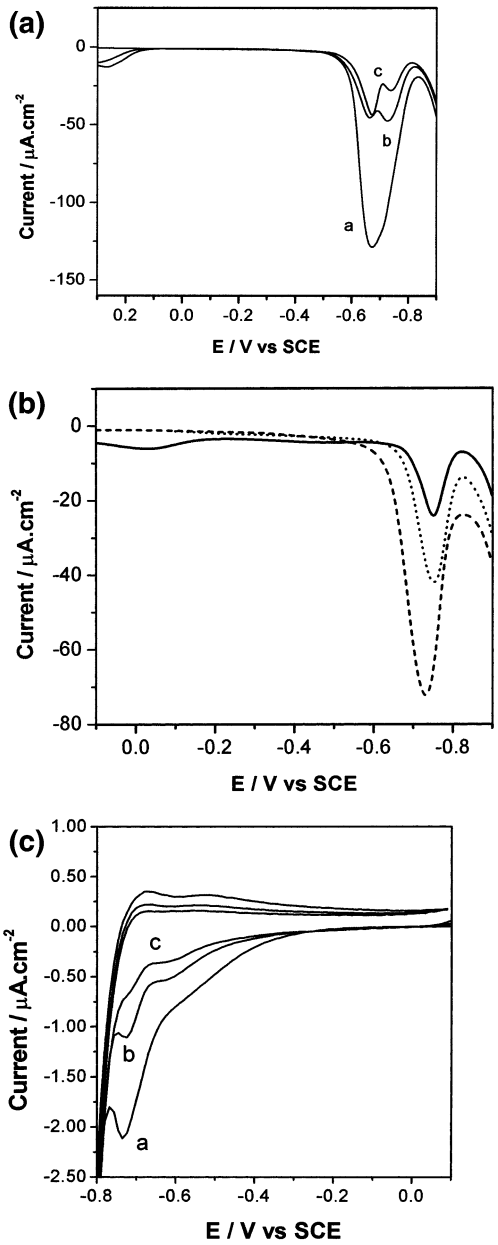

Figure 7. Differential pulse and linear sweep voltammograms for reductive desorption of anchor fragment **11** and the three 4HB-carboprotein forms **6**, **10**, and **12**, from Au(111) in 100 mM phosphate buffer, pH 6.9. Scan rate: 10 mV s^{-1}. (A) Anchor **11**. (a) First scan, (b) second scan, (c) third scan. (B) 4HB carboproteins. Dashed line, 4HB carboprotein **6**; dotted line, 4HB-carboprotein dimer **10**; fully drawn line, 4HB carboprotein without anchor **12**. (C) Three successive linear sweep scans. The peak position in the first scan is at −728 mV. The peak positions of the subsequent sans are shifted to more positive potentials and the peaks become smaller with each scan.

on the negative side (Table 1). This accords with a reductive CV desorption peak at −702 mV reported previously for the anchor **11**.[50] The observation of a well defined desorption peak clearly separate from the onset of dihydrogen evolution is not common for thiol desorption at neutral pH. The two DPV peaks accord, interestingly, with almost equally abundant highly ordered domains and regions of adsorbate structural disorder visible by in situ STM, cf. below. The DPV peak area, calibrated toward the CV, corresponds to a coverage of (1.6 ± 0.3) ×

(49) Chen, Y.-H.; Yang, J. T.; Chau, K. H. *Biochemistry* **1974**, *13*, 3350−3359.

(50) Brask, J.; Wackerbarth, H.; Jensen, K. J.; Zhang, J.; Nielsen, J.U.; Andersen, J. E. T.; Ulstrup, J. *Bioelectrochemistry* **2002**, *56*, 27−32.

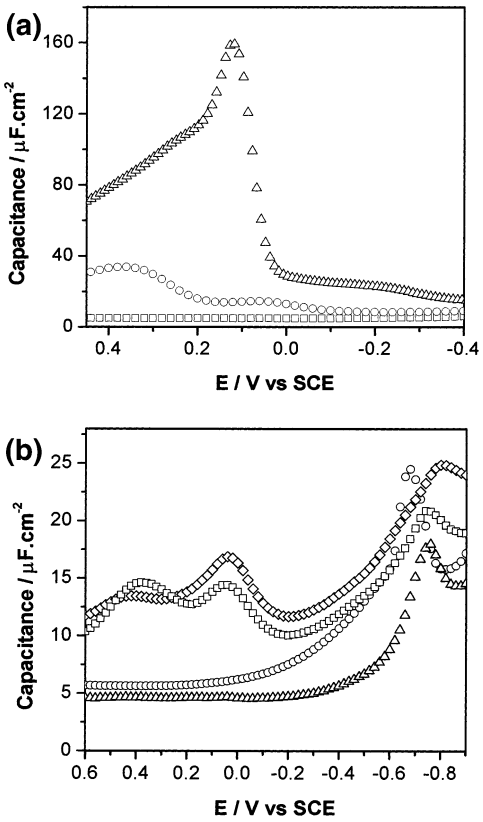

Figure 8. Differential capacitances on adsorption of the three 4HB carboproteins on Au(111) from 100 mM phosphate buffer, pH 6.9. (A) Pure phosphate buffer (△), 4HB carboprotein **6** (□), carboprotein **6** (○) after a single negative potential excursion beyond the reductive desorption potential. (B) Comparison of anchor **11** and 4HB carboproteins **6**, **10**, and **12**. Anchor fragment **11** (○), 4HB-carboprotein dimer **10** (□), 4HB-carboprotein monomer **6** (△), 4HB carboprotein without anchor **12** (◇).

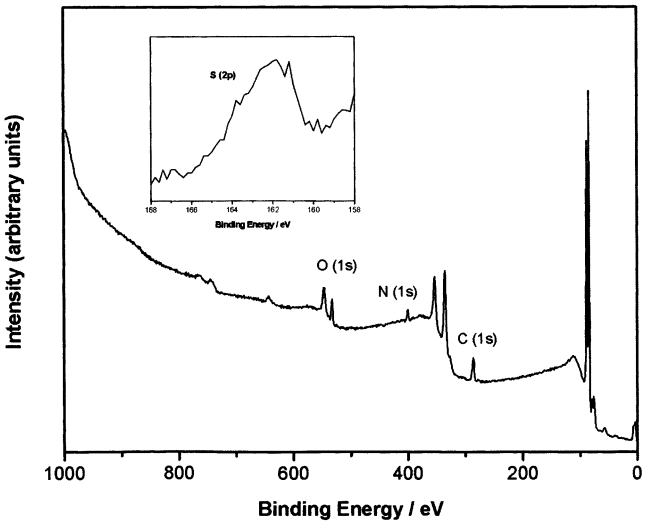

Figure 9. XPS overview spectrum of Au(111) after adsorption of 4HB carboprotein 6. Pass energy 50 eV. (Inset) XPS spectrum in the S(2p) region. Pass energy, 25 eV.

10^{-10} mol cm^{-2}, or close to a monolayer assuming one-electron transfer reductive desorption. Subsequent scans disclose more conspicuous double peaks of decreasing peak areas but in the same potential range. This is different from reductive desorption in strongly basic solution, pH 11.9, where subsequent scans give desorption peaks strongly displaced toward positive potentials.[50] This pattern also resembles reductive desorption of the combined anchor and scaffold fragments.[50] Following conclusions from reported patterns for reductive desorption of nonylthiolate,[51] the different patterns are likely to reflect different concentrations and protonation states of liberated thiol anchor or combined anchor and template fragments. Desorption at high pH liberates deprotonated, negatively charged thiolate, which is repelled from the surface at the high negative potentials. The adsorbate is liberated as electrically neutral protonated thiolate at neutral pH, where the thiol remains in significant concentrations close to the electrode surface and is re-adsorbed much more easily than the thiolate anion.

Figure 7B shows DPV of three different 4HB-carboprotein forms, the thiol monomer **6**, the disulfide dimer **10**, and the sulfur-free carboprotein without anchor **12** (Table 1). All three forms show a peak around −750 mV but the following *differences* are notable:

(1) The peak is by far the highest for the carboprotein monomer **6**. By comparison with the CV (Table 1) the peak area corresponds to $(2.4 \pm 0.4) \times 10^{-11}$ mol cm^{-2} or 40−80% monolayer coverage assuming a 4HB radius of 10−12 Å, cf. below. The peak area for disulfide **10** desorption corresponds to only 30−50% monolayer coverage.

(2) The ratio between the coverages of anchor **12** and 4HB-carboprotein **6** is about 5. This corresponds to an effective radius ratio between the protein and the anchor molecule of 2.2 in the packing on the Au(111) surface. The diameter of the four parallel α-helices on the carbohydrate scaffold is 20−24 Å. The radius of the thiol anchor in extended conformation is between 2.5 and 4 Å, giving a carboprotein/anchor coverage ratio between 6 and 20. The observed ratio is thus on the lower side of the ratio expected from sterically unhindered structures. This could be indicative of lateral attraction in the carboprotein monolayer on the Au(111) surface.

(3) The CV and DPV peak potentials for the 4HB-monomer **6** are −743 and −728 mV, respectively. The peak potentials for 4HB-carboprotein monomer **6** and for dimer **10** are very close (i.e., −743 and −754 mV, respectively). This indicates that disulfide adsorption is accompanied by disulfide bond breaking. The lower coverage may then reflect sterically hindered access and less adsorption of the disulfide form via covalent Au−S bond formation.

(4) Subsequent scans of the adsorbed thiol monomer and disulfide dimer give significantly smaller surface populations but the peaks are largely undistorted. This follows the pattern of the thiol anchor.

(5) The sulfur-free carboprotein **12** *also* gives a voltammetric peak close to the reductive desorption peak of the thiol and disulfide 4HB-carboproteins **6** and **10**. The peak potential is shifted negatively compared with **6** and **10** (i.e., to −759 mV). The peak intensity is the smallest among the carboproteins. There can be two origins of this peak. Oximes and oxime ethers, which are the functionality linking the peptides to the template in carboproteins, are known to undergo irreversible electrochemical four-electron or successive two-electron reductions with cleavage of the N−O bond,[52] in the same potential region as observed here. The data in Figure 7 differ, however, from

(51) Yang, D.-F.; Wilde, C. P.; Morin, M. *Langmuir* **1996**, *12*, 6570−6577.
(52) Kapetanovic, V.; Aleksic, M.; Zuman, P. *J. Electroanal. Chem.* **2001**, *507*, 263−269.

Table 1. Total Charge Determined from DPV and Interfacial Capacitances of the Three 4-α-Helix Bundle Carboproteins and the Thiol Anchor Molecule in the Reductive Desorption Potential Region (First Two Columns)[a]

	peak, mV	DPV, $\mu C \cdot cm^{-2}$	capacitance, $\mu C \cdot cm^{-2}$	%	net charge, $\mu C \cdot cm^{-2}$	coverage, $pmol \cdot cm^{-2}$
4HB-carboprotein monomer **6**	-743 ± 19	3.7 ± 1.4	0.8	20	2.9	30 ± 15
4HB-carboprotein dimer **10**	-754 ± 2	2.4 ± 0.4	0.7	30	1.7	18 ± 4
sulfur-free carboprotein **12**	-759 ± 12	1.3 ± 0.3	0.6	50	0.7	
anchor fragment **11**	-685 ± 18	17.3 ± 3.3	1.6	10	15.7	163 ± 34

[a] "%" indicates the capacitive contribution to the total charge. The fourth column shows the Faradaic contribution and the fifth column the coverage in picomoles per square centimeter.

electrochemical oxime reduction data by involving an adsorbed monolayer, rather than diffusion of bulk oxime. The observation that subsequent scans record a successively decreasing peak at the same potential is also not obviously in keeping with significant irreversible Faradaic oxime reduction. Alternatively the peak could be caused by desorption of "unspecifically adsorbed" sulfur-free carboprotein. This is supported by the interfacial capacitance peak in the same potential range, cf. below. Such a feature would be expected to be far more important for the sulfur-free carboprotein **12** than for the thiol and disulfide forms **6** and **10** at high coverage, where linking of the carboprotein via the thiol anchor will block the access of the helix parts of the carboprotein to the Au(111) surface. Steric hindrance would also block the access of the potentially reducible oxime groups to the surface from other carboprotein fragments.

3.d. Interfacial Capacitance Data. Adsorption of 4HB-carboproteins **6**, **10**, and **12**, and of anchor fragment **11**, as well as the reductive desorption dynamics is reflected in interfacial differential capacitance patterns (Figure 8). The strong peak at 0.1 V is caused by adsorption and desorption of mono- and dihydrogen phosphate ions. The square symbols show the capacitance after adsorption of 4HB-carboprotein **6**. The capacitance has decreased from the peak value of about 130 μF cm^{-2} in pure buffer to less than 10 μF cm^{-2} in the whole potential range. The figure shows, further the differential capacitance after a single negative potential excursion beyond the reductive desorption potential. Partial reappearance of the phosphate adsorption peak is noted, in keeping with the data from DPV. Figure 8B shows the differential capacitances of all the structures, that is, carboproteins **6**, **10**, and **12**, and anchor fragment **11**. Together with the voltammetric data the following observations are notable:

(1) Anchor **11** shows a single strong peak with a peak height of $\approx$25 μF cm^{-2} at the reductive desorption potential compared with a featureless background of $\approx$5 μF cm^{-2}.

(2) All the carboproteins also show a peak close to the DPV peak potentials of reductive desorption, but less intensive than for the anchor **11**. The 4HB-carboprotein monomer **6** shows a lower capacitance than the 4HB-carboprotein dimer **10** and the 4HB-carboprotein **12** without linker. As for the anchor **11**, the monomer **6** also shows a featureless background but weak structural features are apparent at $\approx$0.0 V and $\approx$0.4 V, that is, around the potential of zero charge, for the 4HB-carboprotein dimer **10** and 4HB carboprotein without anchor **12**.

(3) Peak features in the phosphate adsorption region reappear after a negative potential excursion beyond the reductive desorption potential.

3.e. XPS Data. Figure 9 shows a representative overview spectrum in the binding energy range 0−1000 eV of 4HB-carboprotein **6** on Au(111). The carboprotein monolayer gives a marked lowering of the Au(4f) intensity compared with bare Au(111). The bare surface thus discloses 60% Au-atom concentration determined by the intensity of the Au(4f) transition but 30% after carboprotein adsorption, indicative of extensive carboprotein coverage. The atomic composition of the elements C, N, O from the carboprotein stoichiometry and the XPS spectra accord well such as summarized in Table 2. The inset in Figure 9 shows the XPS spectrum in the sulfur 2p region. Although significantly broadened, two peaks at 162.2 and 163.3 eV could always be clearly distinguished. These are characteristic of thiolate headgroup interactions with the gold surface,[38,53,54] and indicative of strong carboprotein adsorption via the thiol anchor.

Table 2. Atomic Concentration of the Elements C, O, and N in Surface-Immobilized 4HB Carboprotein **6** on Au(111) Obtained from XPS

	atomic concentration, %		
	O	N	C
calcd	19.8	14.6	65.6
measd	18.4	12.2	67.2

3.f. In Situ STM of 4HB−Carboprotein Monomer 6 and Anchor Fragment 11. The voltammetric, interfacial capacitance, and XPS data point coherently toward extensive monolayer coverage of the Au(111)-electrode surface either by anchor fragment **11** or full 4HB carboprotein **6** and **10**. This was supported by in situ STM under full electrochemical potential control, directly in the aqueous buffer. In situ STM discloses a monolayer at the *molecular* and *supramolecular* levels. Figure 10A, B shows representative in situ STM images of anchor **11** adsorbed on Au(111) in 10 mM aqueous buffer solution, pH 6.8. Domains of supramolecular organization can clearly be distinguished even though the individual domains do not possess long-range order. A large number of intermediate-size pits (30−50 Å) are also apparent. The domains are oriented in three directions rotated relative to each other and in almost equal abundance. Molecules in each domain seem to be oriented in rows or "pin stripes", illustrated by the height profiles along a given row and perpendicular to a set of rows (Figure 10A). High anchor molecule coverage and significant local structural order thus emerge. The domains are separated by disordered regions in between. As noted the areas of the ordered domains and the disordered domain boundary regions correlated roughly (Figure 7). Figure 10B shows a high-resolution in situ STM image of a monolayer domain of anchor fragment **11**. Different bias

(53) Bain, C. D.; Troughton, E. B.; Tao, Y.-T.; Evall, J.; Whitesides, G. M.; Nusso, R. G. *J. Am. Chem. Soc.* **1989**, *111*, 321−335.
(54) Walcsak, M. M.; Alves, C. A.; Lamp, B. B.; Porter, M. D. *J. Electroanal. Chem.* **1995**, *396*, 103−114.

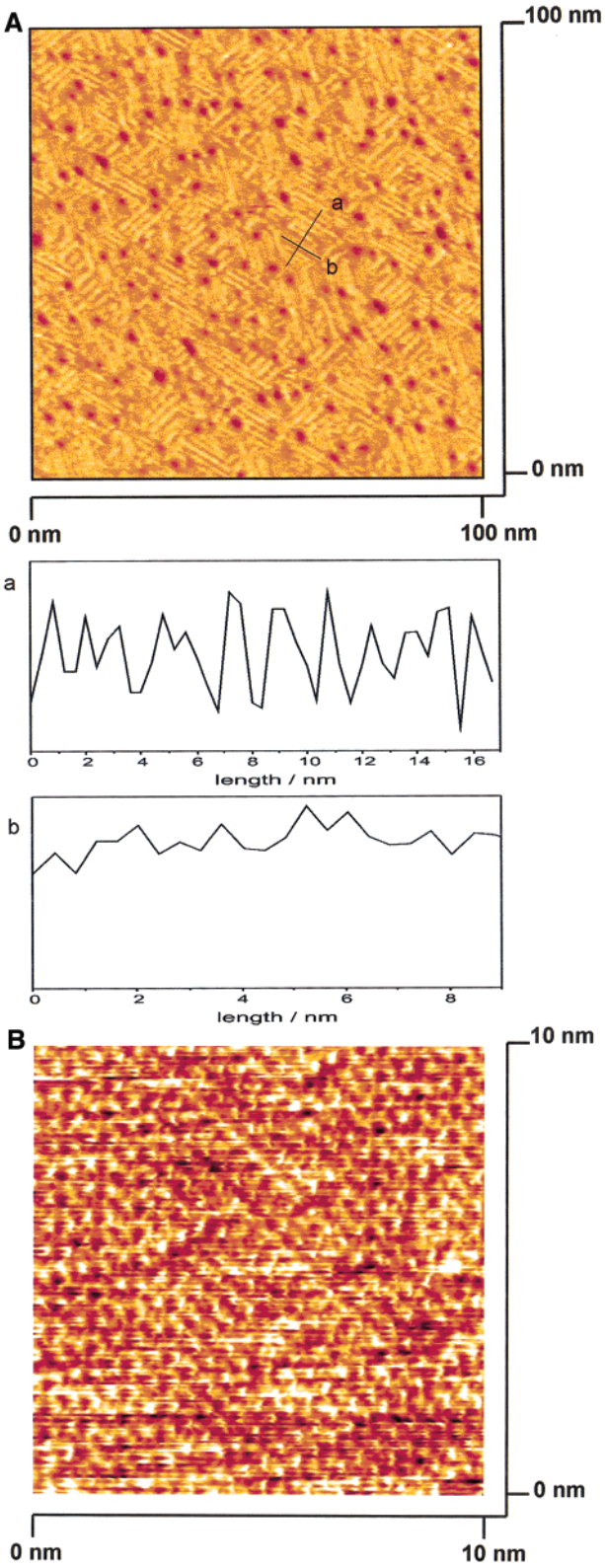

Figure 10. In situ STM of the anchor fragment **11** adsorbed on Au(111), 10 mM phosphate, pH 6.8. Constant current mode. (A) Image area, 100 nm × 100 nm. Tunneling current, 0.3 nA. Sample potential, −460 mV. Bias voltage, 0.2 V. Scan rate, 13 s^{-1}. The height profiles are recorded perpendicular to a set of rows (a) and along a given row (b) indicated by the lines "a" and "b" in the image. (B) Image area 10 nm × 10 nm. Tunneling current, 3 nA. Sample potential, −760 mV. Bias voltage, 0.15 V. Scan rate, 9.8 s^{-1}.

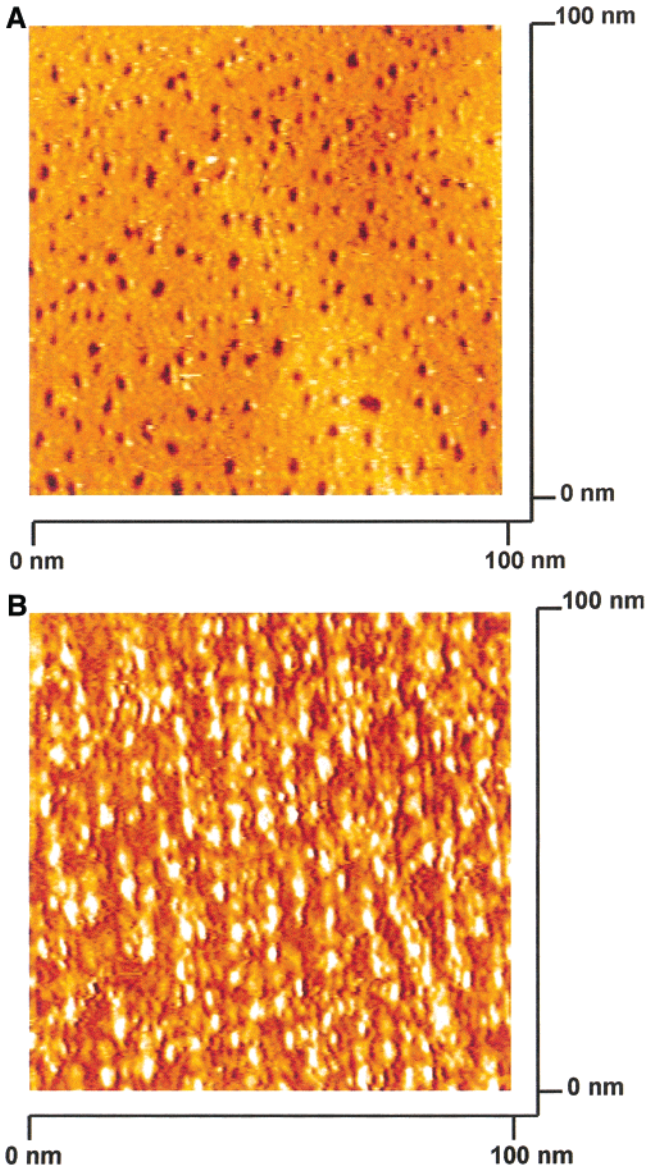

Figure 11. In situ STM images of 100 nm × 100 nm area of 4HB carboprotein **6** adsorbed on Au(111), 10 mM phosphate buffer, pH 6.8. Constant current mode. Tunneling current, 0.3 nA. Scan rate, 9.8 s^{-1}. (A) Sample potential, 0.34 V. Bias voltage, −0.5 V. (B) Sample potential, −0.71 V. Bias voltage, 0.35 V.

potentials, and sample potentials closer to the reductive desorption, cf. below, were here needed for optimal imaging. Both single molecules and the supramolecular striped domain structure can, however, be distinguished.

Figure 11 shows, finally, two in situ STM images of the Au(111)-surface covered by 4HB-carboprotein **6** at two different substrate potentials. Figure 11A is recorded at a potential on the far positive side of the reductive desorption potential. The Au(111)-surface appears fully covered, with the same 30−50 Å pits scattered over the surface as for the anchor fragment **11**. Figure 11B is recorded at a potential, close to the reductive desorption potential. The adsorption pattern here is quite different from the pattern at high potential. Smaller coverage is apparent, with individual single-molecule size structures distinguishable. The controlling in situ STM bias voltage had to be set differently for optimal image quality in the two images, but the "molecular" in situ STM contrasts are noted to disclose

a different *character* close to the reductive desorption potential (Figure 11B) and far from this potential (Figure 11A). A similar but less pronounced difference is apparent for the two images of anchor **11** in Figure 10A, B.

Discussion

The 4HB carboproteins constitute a new class of synthetic proteins with structures based on α-helices mounted on a monosaccharide scaffold.[24−26] Other classes of 4HB synthetic proteins based on peptide templates[27,30,31] and disulfide linking[28,29] have been reported and subjected to extensive physical-chemical characterization. Hence, recently developed chemical methodologies have put model proteins within the reach of synthetic chemistry. Merits of the synthetic proteins are that they hold options for systematic sequence and structure variation, so that the effects of charge, hydrophobic surface patches, ligation, and broad secondary and tertiary structural features become available. In these ways their perspectives differ from those offered by microbiological structure modification (site directed mutagenesis) and from attempts toward total synthesis of natural redox and nonredox proteins,[55−57]which still pose stricter limitations in these respects.

For the purpose of studying proteins adsorbed on gold surfaces, it is desirable that a single thiol or disulfide moiety is present at a specific position in the structure. Except for the very first reported carboprotein, in which the pyranoside aglycon was used to link the structure to a solid phase during synthesis of the four peptide strands,[24] the potential of functionalizing carboproteins at the template aglycon has not previously been utilized.[58] It was envisioned that a thiol anchor at the free aglycon of a carboprotein structure would give adsorption without interference with the folding of the structure. The 4HB-carboprotein monomer, **6**, was prepared based on this strategy. However, as analytical gel filtration result (Figure 4) showed, some degree of air oxidation to the disulfide form was unavoidable. To circumvent the presence of both monomers and dimers, the 4HB-carboprotein dimer, **10**, was assembled on dimeric template **9**. In both cases, chemoselective oxime ligation between the peptide aldehyde and the aminooxy-functionalized template gave the desired carboprotein in quantitative yield and high purity, as judged by HPLC and MS (Figure 3). Previous studies of the 4HB carboprotein without thiol anchor, **12**, have indicated that the four peptide strands on the d-Gal*p* template do interact to form a bundle structure.[41] Hence, it is reasonable to assume that carboprotein **6**, which only differs from **12** in the aglycon, forms a similar 4HB structure. Likewise with the dimeric structure **10**, although it is uncertain if this carboprotein forms two 4HB structures or if all peptide strands interact to form a 8HB structure. The CD spectra of **6** and **10** supported the hypothesis of bundle structures as both carboproteins were found to be highly α-helical (Figure 5). Because sample concentrations were determined gravimetrically on milligram quantities of material, there are some uncertainties as to the exact amount of α-helix in the structures, calculated to 57% and 61% for **6** and **10**, respectively. In a previous study, the helicity of carboprotein **12** was calculated to 64%.[41]

Natural and synthetic redox proteins hold exciting perspectives in new biotechnology, approaching control of biotechnological function at the nanoscale and single-molecule levels. Prerequisites are that the proteins can be immobilized in ordered functional states on well-defined solid substrates, which also interface to electrical, mechanical, and other external circuits. In this report we have shown that 4HB proteins can be brought to immobilization on single-crystal, atomically planar Au(111) surfaces. CV, DPV, interfacial capacitance, and XPS data have mapped a coherent pattern of close to monolayer coverage of both 4HB carboprotein **6** and thiol anchor **11**. The protein monolayer is functional in the sense that the proteins chemisorbed via covalently attached thiol anchors display the expected features of well-defined Au−S bond formation. The disulfide 4HB-carboprotein dimer **10** is adsorbed in the same potential range, but the peak area is much smaller. The carboprotein without linker **12** shows a peak at the lowest potential and has the smallest peak area of the three carboproteins. The reductive desorption peak of the thiol 4HB-carboprotein monomer **6** is therefore also likely to hold a capacitive component (Table 1).

We have, further, obtained in situ STM images of both the adsorbed anchor **11** and the full 4HB carboprotein **6**. The resolution discloses both supramolecular organization and single-molecule features, which has not been reported previously for 4HB proteins. The in situ STM data also define electrochemical potential ranges of adsorbed monolayer stability. In situ STM of redox and nonredox proteins under full potentiostatic control is, further, still novel and has only been reported in a very few cases.[32−38,59] The anchor fragment **11** forms monolayers with lateral domain order but small lateral extension of the individual domains. The domains extend in three different directions oriented 60° relative to each other and separated by almost equally abundant interdomain regions. This accords with two peaks in the DPV for reductive desorption of roughly the same intensity ratio. 4HB carboprotein **6** clearly forms dense monolayers but without lateral order such as for anchor **11**. Lack of two-dimensional lateral order is a common observation in the, still very few, reported cases of in situ STM of biological macromolecules. The character of the monolayer and imaging contrast changes drastically as the electrochemical potential for reductive desorption is approached. A decrease in the coverage is clearly distinguishable, accompanied by increased apparent spatial resolution toward the single-molecule level. The in situ STM *contrast* also changes toward strongly enhanced tunneling. With reference to recent theoretical approaches to molecular in situ STM mechanisms,[60−62] it could be suggested that different in situ STM tunneling channels are operative close to the reductive desorption potential and far from this potential. Electron tunneling far from reductive desorption is effected by superexchange via the lowest unoccupied molecular orbital (LUMO) of the molecular adsorbate. This level is far off resonance relative to the Fermi levels of the substrate and tip in these potential ranges. As the Au(111) substrate potential approaches the reductive desorption potential, the LUMO is

(55) Christensen, H. E. M.; Hammerstad-Pedersen, J. M.; Holm, A.; Iversen, G.; Jensen, M. H.; Ulstrup, J. *Eur. J. Biochem.* **1994**, *224*, 97−101.
(56) Hellinga, H. W.; Marvin, J. S. *Trends Biotechnol.* **1998**, *16*, 183−189.
(57) Kennedy, M. L.; Gibney, B. R. *Curr. Opion. Struct. Biol.* **2001**, *11*, 485−490.
(58) Jensen, K. J.; Brask, J. *Cell. Mol. Life Sci.* **2002**, *59*, 859−869.
(59) Andolfi, L.; Cannistrarro, S.; Canters, G. W.; Facci, P.; Ficca, A. G.; Van Amsterdam, I. M. C.; Verbeet, M. P. *Arch. Biochem. Biophys.* **2002**, *399*, 81−88.
(60) Kuznetsov, A. M.; Sommer-Larsen, P.; Ulstrup, J. *Surf. Sci.* **1992**, *275*, 52−64.
(61) Friis, E. P.; Kharkats, Y. I.; Kuznetsov, A. M.; Ulstrup, J. *J. Phys. Chem. A* **1998**, *102*, 7851−7859.
(62) Kuznetsov, A. M.; Ulstrup, J. *J. Phys. Chem. A* **2000**, *104*, 11531−11540.

brought close to the Fermi level of the Au(111) electrode and now mediates in situ STM by temporary LUMO population and depopulation. This enhances tunneling significantly. Unfortunately, the expected *reversible* dependence of this effect cannot be tested due to the significant adsorbate depopulation which accompanies the redox process.

Heme groups and blue copper-center binding to synthetic 4HB proteins has been extensively reported recently and characterized spectroscopically and voltammetrically.[28,29,63−65] The 4HB carboproteins offer similar options, but our approach has differed somewhat from the previous reports. We have, first, exploited a comprehensive, state-of-the-art physical electrochemical approach. A primary basis has been the use of bead and disk Au(111) electrodes. The surfaces of these electrodes are atomically planar over up to several hundred nanometers. The single-crystal electrodes have been combined with electrochemical (CV, DPV, and capacitance measurements) and spectroscopic (XPS) characterization, with focus on the Au−S bonding and electrode coverage of adsorbed carboprotein and anchor structures. The single-crystal electrochemical approach has, secondly, paved the way for addressing the adsorbate monolayers by in situ STM toward the *single-molecule* level. Single-molecule resolution has been achieved for both the anchor fragment **11** and the full 4HB carboprotein **6**, but only the former shows supramolecular order on the Au(111) surface. Different in situ STM contrasts can, further, be distinguished in electrochemical potential ranges far from the reductive desorption potential and close to this potential.

The primary target molecules of our investigation, the 4HB carboproteins, do not hold a metal redox center. Histidines and other residues suitable for heme group attachment can, however, be inserted into the carboproteins similar to other 4HB structures.[27−31] The hydrophobic heme group could *also* be trapped by noncovalent hydrophobic interactions in the space between the four organized α-helices, which have been designed with a hydrophobic interior and a hydrophilic surface in contact with the outer aqueous solution. Such a confinement would endow the enclosed heme group with considerable internal mobility. This would detract from options of addressing electron transfer *distances* and related notions in electron transfer theory[66] but hold other favorable perspectives relating to efficient electronic transmission in the in situ STM mode and more broadly, toward working biosensor function. A mobile heme group could thus efficiently both accept and donate electrons at short distances from the substrate electrode and tip, if these two steps were separated by internal translation. Work along these lines is in progress.

Acknowledgment. Financial support from The Danish Technical Science Research Council (grant 26-00-0034) is acknowledged.

JA020943R

(63) Chen, X. X.; Discher, B. M.; Pilloud, D.L.; Gibney, B. R.; Moser, C. C.; Dutton, P. L. *J. Phys. Chem. B* **2002**, *106*, 617−624.
(64) Katz, E.; Heleg-Shabtai, V.; Bardea, A.; Willner, I.; Rau, H.; Haehnel, W. *Biosens. Bioelectron.* **1998**, *13*, 741−756.
(65) Shifman, J. M.; Gibney, B. R.; Sharp, R. E.; Dutton, P. L. *Biochemistry* **2000**, *39*, 14813−14821.
(66) Kuznetsov, A. M.; Ulstrup, J. *Electron Transfer in Chemistry and Biology. An Introduction to the Theory*; Wiley: Chichester, UK, 1999.